PCCP

Accepted Manuscript

ROYAL SOCIETY OF CHEMISTRY

www.rsc.org/pccp

Roles of Water Molecules in Trapping Carbon Dioxide Molecules inside the Interlayer Space of Graphene Oxides

Takashi Yumura* **and Ayumi Yamasaki**

Department of Chemistry and Materials Technology, Kyoto Institute of Technology, Matsugasaki, Sakyo-ku, Kyoto, 606-8585, Japan

*To whom all correspondence should be addressed. E-mail; yumura@chem.kit.ac.jp

Abstract: Density functional theory (DFT) calculations were employed to investigate the energetics of carbon dioxide migration within hydrated or anhydrous graphene oxides (GOs). When anhydrous GO structures contain a carbon dioxide molecule, the carbon dioxide interacts repulsively with the GO layers to increase the interlayer spacing. The repulsive electrostatic interactions are reduced by the insertion of water molecules into CO_2-containing GO structures due to the occurrence of attractive water–layer interactions through hydrogen bonding. Consequently, the interlayer spacings in CO_2-containing hydrated structures are shortened compared with those in the anhydrous structures. The results indicate that the intercalated water molecules have the ability to connect the GO layers in the presence of carbon dioxide. Furthermore, the DFT calculations indicated that the GO interlayer spacings, which are influenced by the intercalation of water molecules, control carbon dioxide migration within the GO layers. The importance of the interlayer spacings on the migration of carbon dioxide arises from the occurrence of repulsive interactions between CO_2 and oxygen-containing groups attached on the graphene sheets. When the GO interlayer spacings are short due to the presence of intercalated water molecules, the repulsive interactions between carbon dioxide and the GO layers are strong enough to prevent CO_2 from migrating from its original position. Such repulsive interactions do not occur during the migration of CO_2 within anhydrous GO structures because of the relatively longer interlayer spacing. Accordingly, CO_2 migrates within anhydrous GO with a less significant barrier, indicating that carbon dioxide molecules are easily released from the GO.

Introduction

Graphite oxides are generated via oxidation treatment of graphite under various conditions.[1–8] The few layers within these structures, graphene oxides (GO), have attracted attention from many researchers[9–11] because of their use for the mass production of graphene [12,13] and because of their unique electronic properties that can be tuned by the degree of oxidation.[14–21] To understand the structure–functionality relationships of graphene oxides, state-of-the-art techniques have been employed.[22–35] Although the structural features of GOs have been debated, there is a consensus that various types of oxygen-containing groups, such as epoxy, hydroxyl and carboxyl groups, are bound to graphene sheets to disrupt the sp^2 frameworks.

The presence of the oxygen-containing groups weakens the van der Waals forces between the graphene sheets. Rather than van der Waals forces, hydrogen-bonding interactions occur between the functional groups attached to the adjacent layers. Consequently, the spacing between adjacent GO layers is increased relative to that in graphite (3.35 Å). Another important factor in determining the interlayer spacings is the intercalation of water molecules.[36–38] The affinity to water molecules is a consequence of the presence of hydrogen bonding with the oxygen-containing groups attached to the graphene surface. The intercalation of water further enhances the interlayer spacings in GO structures compared with those in anhydrous structures.[22–24] According to Ref. 24, the interlayer spacings in the hydrated GO structure range from 5.6 to 12 Å depending on water content. As a result, the chemistry of GO layers is strongly sensitive to humidity.

Because of their layered structures, GOs have the potential to capture gases such as dihydrogen[39,40] and carbon dioxide.[37,41] We are interested in how carbon dioxide molecules are trapped between GO layers because of environmental concerns. According to the Fourier transform infrared (FT-IR) measurements in Refs. 37 and 41, carbon dioxide is formed during the thermal treatment of GO films. Subsequently, the resultant carbon dioxide molecules are intercalated between the GO layers. Thermogravimetric analyses (TGA) combined with mass- and IR-spectrometers (TGA-MS and TGA-IR) indicated that the CO_2-intercalated GO structures are stable up to 120°C. The intercalated carbon dioxide molecules are released at approximately 160°C by decomposition of the GO structures. Interestingly, the removal of CO_2 is accompanied by the release of water molecules from the GO layers. Therefore, one expects that water molecules have important roles in trapping carbon dioxide molecules in the interlayer spaces of graphene oxides.

Despite the interesting experimental reports, our knowledge on the mechanisms of trapping carbon dioxide molecules in the GO interlayer space, as well as the roles of water molecules in the trapping of carbon dioxide, is still lacking. To increase our understanding on this topic, quantum chemistry calculations,[42–57] especially density functional theory (DFT) calculations, provide useful information. By utilising DFT calculations with periodic boundary conditions, the present study focuses on carbon dioxide migration in the interlayers of hydrated or anhydrous GO structures, which is one event during the release of trapped carbon dioxide.

1. Calculation Method

DFT calculations implemented in the Gaussian 09 code[58] were employed to investigate the structures of anhydrous and hydrated graphene oxides consisting of a double-honeycomb layer. To obtain geometrical information on the double-layered graphene oxides, DFT calculations were performed under periodic boundary condition. As shown in Figure 1, the supercells contain 16, 32, and 64 carbon atoms, corresponding to 2×2×2, 2×4×2, and 4×4×2 cells of graphene, respectively. By using the small and medium supercells corresponding to the 2×2×2 and 2×4×2 cells, respectively, we first added a few hydroxyl groups to the graphene models to construct graphene oxides. After obtaining the graphene oxide structures, one carbon dioxide molecule was inserted into the interlayer space of a certain GO structure whose interlayer spacing was sufficiently large to accommodate CO_2 molecules. To investigate the behaviours of carbon dioxide on the inside of the graphene oxides, we used the large unit cell that contained 64 carbon atoms (4×4×2 cell). In PBC optimization of the two dimensional systems, we used *k*-point meshes that were automatically generated in the Gaussian program (18×18 *k*-point mesh for the small supercell, 10×18 *k*-point mesh for the medium supercell, and 10×10 *k*-point mesh for the large supercell). The 10×10 k-point mesh is sufficient to converge the total energy of a GO model in the larger unit cell, as shown in supporting information.

In anhydrous and hydrated GOs, hydrogen bonding interactions are key in determining their layer structures.[38] To explore the feasibility of using DFT calculations to describe the hydrogen bonds, we considered the PBE functional[59] and the

B97D functional, in which a dispersion correction is included.[60] By using the different functionals, we obtained the local minimum of a water dimer with C_s symmetry, as well as one water molecule that attached to two OH groups on the graphene sheet. Here, the 6-31G**[61] and 6-31++G**[62] basis sets were used. The optimised structures are displayed in Figure 2, and key parameters of these structures (hydrogen bonding separations and its stabilization energy) are shown in Table 1. In the optimised structure for the water dimer, one hydrogen bond is formed between an H atom of one water molecule with the O atom of the other molecule. The HOH··OH separations are approximately 1.91 Å, and they are not sensitive to the considered functionals (PBE or B97D) or to whether diffuse functions are used. Subsequently, we evaluated the stabilisation energies by the dimer formation, as tabulated in Table 1. Table 1 indicated that the stabilisation energies were also independent of the functionals and basis sets that we considered. Note that the calculated stabilisation energies, especially the PBE values, are consistent with previously reported experimental values.[64] This consistency, which has also been reported by several researchers,[65-67] indicates that the PBE functional is the best functional for describing the hydrogen-bonding interactions. We also investigated the addition of one water molecule into a single GO layer using the two functionals.[68] Table 2 lists the two key parameters that are the basis for understanding the behaviours of water molecules within double GO layers, which will be discussed below. As can be seen in Table 2, there is similarity between the B97D and PBE calculations in the key parameters,[69] although the stabilization energy in the B97D calculation was less significant than the PBE case. Similar trend was found

from Figure 2 and Table 2 in interactions of a single OH-attached graphene with CO_2. The results indicate that the dispersion corrections in the B97D functional are not important in describing hydrogen-bonding interactions in both systems.

Considering the above discussion, we chose the PBE functional to describe hydrogen-bonding interactions in the following. With respect to the basis sets, Tables 1 and 2 also shows that the PBE/6-31G** calculations provide results that are qualitatively similar to those from the PBE/6-31++G** calculations. Due to limited computational resources, we cannot use the 6-31++G** basis sets. Instead, the 6-31G** basis sets were employed. Our previous studies[70] have shown that DFT calculations with the 6-31G** basis sets are sufficiently accurate for reproducing the experimental data of nanocarbon materials.

2. Results and Discussion

2.1. Structural Features of Graphene Oxides with Different Degrees of Oxidation

First, we discuss the interlayer spacings in double GO layers with different degrees of oxidation. In these analyses, we used smaller supercells containing 16 or 32 carbon atoms with some attached hydroxyl groups. After conducting the DFT calculations, the local minima of these structures were obtained, as shown in Figure 3. The optimised structures in Figure 3 have hydrogen bonds, which are indicated by dotted lines. There are various types of hydrogen bonds, which are schematically depicted in Chart 1. With the exception of the $C_{16}(OH)_6$ structure, the optimised

structures have interlayer hydrogen bonds: accepter oxygen atoms on a layer are connected to donor hydrogen atoms of OH groups on the other layer (Chart 1a), with hydrogen bond lengths ranging from 1.8 to 2.5 Å. In addition, intralayer hydrogen bonds were found in the $C_{16}(OH)_4$, $C_{32}(OH)_4$, and $C_{32}(OH)_6$ structures (Chart 1b), whose ratios of the number of oxygen atoms to that of carbon atoms ([O]/[C]) are 0.125 ~ 0.25. Figure 3 and Table 3 show that the computed interlayer spacings increase as increasing the [O]/[C] values.[71] Our DFT calculations are similar to those that have previously been reported in Refs. 45 and 50.

In graphene with a high degree of oxidation, slightly different structural features were observed, as shown in Figure 3. The $C_{16}(OH)_6$ structure ([O]/[C] = 0.375) contains one water molecule, which was generated during the optimisation process where the H atom of an OH group migrates toward the adjacent OH group. Concurrently, one epoxy group was formed on a layer. The optimised structure ($C_{16}O(OH)_4 \cdot H_2O$) has hydrogen bonds mediated by the water molecule, and these bonds range from 2.02 to 2.46 Å. In these hydrogen bonds, the two hydrogen atoms of a water molecule point towards oxygen atoms attached to graphene, and at the same time, the water oxygen atom is bound to the hydrogen atom of an attached hydroxyl group, as shown in Chart 1c. Negative charges on the oxygen atoms are important for forming the hydrogen bonds.[72] Due to the presence of water molecules between the GO layers, the structure has a relatively long interlayer spacing (d = 7.08 Å). In terms of intralayer hydrogen bonding, chain-like orientations were found, being similar to those reported in Ref. 53. Ref. 73 indicates that such chain-like orientations are preferable to

amorphous orientations. Based on previous experimental reports,[37,41] we hypothesise that water molecules play an essential role in controlling the migration behaviours of intercalated carbon dioxides. Thus, the hydrated structure with a relatively large interlayer spacing is the simplest model that provides us with a preliminary idea for elucidating the roles of water molecules in trapping carbon dioxide molecules within GO layers.

2.2. Carbon Dioxide in the Interlayer Space of Graphene Oxides

In this section, we examine the behaviours of a carbon dioxide molecule that is present in the interlayer space of graphene oxides. For this purpose, we quadrupled the $C_{16}O(OH)_4 \cdot H_2O$ structure (Figure 3c) to construct $C_{64}O_4(OH)_{16} \cdot 4H_2O$, whose side and top views are shown in Figures 4(a) and 4(b), respectively. There are four water molecules present in the 4×4×2 cell. The neighbouring oxygen atoms between adjacent water molecules are separated by 5.02 Å, as shown in Figure 4(c). Because the oxygen separation in carbon dioxide is 2.36 Å, the space surrounded by the four water molecules is too small to accommodate one carbon dioxide molecule. To trap one carbon dioxide molecule between the GO layers in this model, we removed some water molecules from the $C_{64}O_4(OH)_{16} \cdot 4H_2O$ structure to construct $C_{64}O_4(OH)_{16} \cdot nH_2O$ structures. Here, the number of water molecules (n) ranges from 0 to 3. Then, we placed carbon dioxide into the interlayer of the $C_{64}O_4(OH)_{16} \cdot nH_2O$ structures. By using the initial $C_{64}O_4(OH)_{16} \cdot nH_2O$ and $CO_2@C_{64}O_4(OH)_{16} \cdot nH_2O$ geometries, we obtained local minima.

2.2.1. Structural Features of $C_{64}O_4(OH)_{16}\cdot nH_2O$

First, let us focus on how the structural features of $C_{64}O_4(OH)_{16}\cdot nH_2O$ depend on the number of water molecules. Figure 5 displays the optimised geometries for the $C_{64}O_4(OH)_{16}\cdot nH_2O$ structures. The anhydrous GO structure ($C_{64}O_4(OH)_{16}$) has a stacking behaviour that slightly deviates from AA stacking. The observed stacking behaviour is 5.5 kcal/mol more stable than the corresponding AB stacking.[74] As mentioned above, oxygen-containing groups are connected by hydrogen bonds between adjacent GO layers (*l*). Here, we evaluated interaction energies due to the interlayer hydrogen bonds, $E(l–l)$, defined in the following,

$$E(l–l) = E_{\text{total}}([C_{64}O_4(OH)_{16}]') - E_{\text{total}}(\text{top layer of } [C_{64}O_4(OH)_{16}]') - E_{\text{total}}(\text{bottom layer of } [C_{64}O_4(OH)_{16}]')$$

where $[C_{64}O_4(OH)_{16}]'$ is the $C_{64}O_4(OH)_{16}$ structure taken from an optimised $C_{64}O_4(OH)_{16}\cdot nH_2O$ structure, $E_{\text{total}}([C_{64}O_4(OH)_{16}]')$ is the total energy of the $[C_{64}O_4(OH)_{16}]'$ structure, and $E_{\text{total}}(\text{top layer of } [C_{64}O_4(OH)_{16}]')$ or $E_{\text{total}}(\text{bottom layer of } [C_{64}O_4(OH)_{16}]')$ is that of the top or bottom layer taken from the $[C_{64}O_4(OH)_{16}]'$ structure. BSSE-corrected $E(l–l)$ values are listed in Table 4. The negative $E(l–l)$ value in the anhydrous structure indicates that the two layers interact attractively through interlayer hydrogen bonds.

In contrast to the anhydrous GO structure, different stacking behaviours were observed in the hydrated structures (Figure 5). In these situations, water molecules strongly interact with the GO layers through hydrogen-bonding interactions. In fact, the water molecules orient their H atoms towards the oxygen atoms of epoxide or hydroxyl groups on GO. In addition to the interlayer hydrogen bonds, interactions of water molecules with a GO layer are responsible for determining the hydrated structures. Figure 6 shows that the interlayer spacings increase as the number of intercalated water molecules increases. The results suggest that direct interlayer hydrogen-bonding interactions would be weakened by the insertion of water. Instead, the interactions of water molecules with the GO layers would become dominant. To quantitatively determine these changes in terms of the interactions, we evaluated the water–layer interaction energies ($E(w–l)$) and then compared them with the corresponding $E(l–l)$ values, as shown in Table 4. The $E(w–l)$ values are defined as follows,

$$E(w–l) = (E_{total}(C_{64}O_4(OH)_{16}\cdot nH_2O) – nE_{total}(H_2O) – E_{total}(C_{64}O_4(OH)_{16})) / n$$

where $E_{total}(C_{64}O_4(OH)_{16}\cdot nH_2O)$ is the total energy of an optimised $C_{64}O_4(OH)_{16}\cdot nH_2O$ structure and $E_{total}(C_{64}O_4(OH)_{16})$ and $E(H_2O)$ are those of $C_{64}O_4(OH)_{16}$ and water molecules taken from the optimised $C_{64}O_4(OH)_{16}\cdot nH_2O$ structure, respectively. As shown in Table 4, the calculated $E(w–l)$ values are approximately –10 kcal/mol. The negative $E(w–l)$ values indicate that attractive interactions occur between water molecules and the two GO layers.

Based on the $E(l–l)$ and $E(w–l)$ values in Table 4, the water–layer interactions are dominant in the hydrated GO structures. The importance of the water-layer interactions arises from the formation of a large number of hydrogen bonds, as shown in Figure 5. When some number of water molecules exist within the layers, hydrogen bonding networks in Chart 1c are created to gain the stabilisation energy due to the water–layer interactions. Then, the water–layer interactions are strong enough to change the GO stacking pattern. In contrast, the $C_{64}O_4(OH)_{16}·H_2O$ structure, whose interlayer spacing is relatively short, has a slightly different orientation of intercalated water molecules in Chart 1d. In this situation, interlayer hydrogen bonds influence the orientations of water molecules within the GO layers. Therefore, the interlayer-hydrogen interactions are also a key in determining the $C_{64}O_4(OH)_{16}·H_2O$ structure, in addition to the water-layer interactions.

2.2.2. Carbon Dioxide in the Interlayer Space of Graphene Oxides

When carbon dioxide exists in the interlayer space of graphene oxides, the state of affairs is slightly different in terms of the structural and energetic features in Figure 7. As shown in Figures 5 and 7, the presence of carbon dioxide within the GO layers significantly enhances the interlayer spacing. In particular, long interlayer spacing was found in $CO_2@C_{64}O_4(OH)_{16}$ (8.45 Å). The two oxygen atoms of carbon dioxide have negative charges, and at the same time, negative charges exist on the oxygen atoms attached to the GO layers.[72] The repulsive electrostatic interactions between the

negatively charged oxygen atoms are counteracted by the enhancement of the interlayer spacing. The interactions of CO_2 with the GO structures were evaluated as follows,

$$E(CO_2\text{–}l) = E_{total}(CO_2@C_{64}O_4(OH)_{16}\cdot nH_2O) - E_{total}(CO_2) - E_{total}(C_{64}O_4(OH)_{16}\cdot nH_2O),$$

where $E_{total}(CO_2@C_{64}O_4(OH)_{16}\cdot nH_2O)$ is the total energy of an optimised $CO_2@C_{64}O_4(OH)_{16}\cdot nH_2O$ structure and $E_{total}(C_{64}O_4(OH)_{16}\cdot nH_2O)$ and $E_{total}(CO_2)$ are the total energies of $C_{64}O_4(OH)_{16}\cdot nH_2O$ and CO_2, respectively, taken from the optimised $CO_2@C_{64}O_4(OH)_{16}\cdot nH_2O$ structure.

Less significant $E(CO_2\text{–}l)$ values are observed in Table 4, indicating that the interactions between CO_2 and the GO layers are quite weak. In particular, the CO_2-containing hydrated GO structures have positive $E(CO_2\text{–}l)$ values, indicating that repulsive interactions occurred between CO_2 and the GO structures. Relatively large separations between the oxygen atoms were observed in the CO_2-containing GO structures, and thus, the weak repulsive interactions are understandable. Within the hydrated cases, the weak repulsion is easily counteracted by attraction by the water–layer interactions. Consequently, the interlayer spacings in $CO_2@C_{64}O_4(OH)_{16}\cdot nH_2O$ are smaller than those in $CO_2@C_{64}O_4(OH)_{16}$. Table 4 indicates that the water–layer interactions are a dominant factor for determining the $CO_2@C_{64}O_4(OH)_{16}\cdot nH_2O$ structures. Consequently, water molecules have the ability to connect adjacent GO layers in the presence of carbon dioxide. This ability of the intercalated water

molecules is important in controlling the migration of carbon dioxide in the interlayer of the GO structures, as will be discussed below.

2.2.3. Migration of Carbon Dioxide in the Interlayer Space of GO Structures

The previous section revealed that substantial attraction does not occur between carbon dioxide and the double graphene oxides. Unfortunately, the DFT findings cannot explain the trapping of carbon dioxide in the interlayer space, which was experimentally reported in Refs. 37 and 41. To increase our understanding of the mechanism for CO_2 trapping, we consider how carbon dioxide migrates within the double GO layers in the presence or absence of intercalated water molecules. Here, we scanned the total energy of the migration of CO_2 along the (a_1+a_2) axis of the graphene oxide structure, as shown in Figure 8. The degree of CO_2 migration from the original structure is defined as T. The original structure, which corresponds to the optimised $CO_2@C_{64}O_4(OH)_{16}\cdot nH_2O$ structure, is at T = 0 Å. During CO_2 migration, the $C_{64}O_4(OH)_{16}\cdot nH_2O$ structure is fixed to that taken from the optimised $CO_2@C_{64}O_4(OH)_{16}\cdot nH_2O$ by removing CO_2, and the orientation of CO_2 with respect to the two layers (in particular, its height (z coordination)) is maintained constant. Figure 9 shows energy profiles for the migration of CO_2 within the $C_{64}O_4(OH)_{16}\cdot nH_2O$ structure. By scanning the total energies in Figure 9, we obtained the transition states of the $CO_2@C_{64}O_4(OH)_{16}$ and $CO_2@C_{64}O_4(OH)_{16}\cdot nH_2O$ structures at T = 3.2 and 2.6 Å, respectively. As shown in Figure 9, the activation energy for CO_2 migration (E_a) is

sensitive to the number of water molecules; the E_a values decrease from 44.0 to 8.4 kcal/mol when n decreases from 2 to 0.[75]

The energy barrier is caused by CO_2 exerting repulsive interactions with water molecules and with oxygen-containing groups attached to graphene sheets. As shown in Figure 10, the transition state has the oxygen atoms of carbon dioxide separated from the oxygen atoms of the water molecules by approximately 3.4 Å and from the oxygen atoms of functional groups on the GO layers by 2.2 Å. Their oxygen separations were shorter than those in the corresponding original structures (T = 0 Å), as shown in Figures 7 and 10. Because the oxygen atoms in CO_2, H_2O, and the functional groups have negative charges, repulsive electrostatic interactions occur in the transition states.

In terms of the repulsive interactions occurring in the transition states, water molecules play two roles. One role is that water molecules directly repel carbon dioxide through electrostatic interactions. The other role is that water molecules connect the two GO layers through hydrogen bonds. The two layers being closely separated strongly repel the intercalated carbon dioxide. Thus, the spacings between the adjacent GO layers, which are connected by water molecules, become essential in determining how strong repulsive interactions operate between CO_2 and GO layers. At a short interlayer spacing, carbon dioxide is close to the oxygen atoms of the attached functional groups. Then, the migration of CO_2 is strongly hindered by oxygen-containing groups through their repulsive interactions. This situation can be observed in the $CO_2@C_{64}O_4(OH)_{16}\cdot 2H_2O$ structure, whose interlayer spacing is 7.70 Å. In contrast, the anhydrous graphene oxide has an interlayer spacing of 8.45 Å. The

spacing is too long to exert repulsive interactions between CO_2 and oxygen-containing functional groups. Therefore, the smaller activation energy for CO_2 migration (8.0 kcal/mol) in the anhydrous GO is reasonable. The DFT calculations revealed that the kinetics for CO_2 migration within graphene oxides layers are influenced by the number of intercalated water molecules. Accordingly, we proposed from the DFT calculations that water molecules play an important role in effectively trapping carbon dioxide molecules.

The DFT findings are directly linked to the experimental reports in Refs. 37 and 41. When water molecules exist in the interlayer space of graphene oxides, the migration of carbon dioxide molecules is hindered, as our DFT findings indicate that the molecules are trapped in the interlayer space. According to Refs. 37 and 41, heat treatments release water molecules from the GO interlayer space, which occurs concomitantly with the removal of carbon dioxide. The experimental findings can be well interpreted based on our DFT findings because we found that the release of water enhances the GO interlayer spacings, allowing the inner carbon dioxide molecules to move easily and finally be released. Consequently, the intercalated water molecules would control the migration of carbon dioxide molecules within the graphene oxide layers, which is key for graphene oxides to capture carbon dioxide molecules in their interlayer space.

Conclusions

We employed density functional theory (DFT) calculations under periodic boundary conditions to investigate how carbon dioxide migrates in the interlayer space of hydrated or anhydrous graphene oxides (GOs). First, we obtained information on the geometrical features of the anhydrous and hydrated structures. The DFT calculations revealed that interlayer hydrogen-bonding interactions and water–layer interactions are responsible for determining the layer structures of GOs. When a carbon dioxide molecule is present in the anhydrous GO structure, the intercalated CO_2 repels the GO layers through electrostatic interactions to separate adjacent GO layers, compared with the pristine case. The repulsive electrostatic interactions are counteracted by the insertion of water molecules because attractive interactions occur between the water molecules and GO layers. In fact, the insertion of water into CO_2-containing GO structures decreases their interlayer spacings. Accordingly, the intercalated water molecules have the ability to connect the CO_2-intercalated GO structures.

Furthermore, the presence of intercalated water molecules strongly influences the migration of carbon dioxide within GO layers. When intercalated water molecules are present in CO_2-containing GO structures, their interlayer spacings are relatively smaller than in the anhydrous structures. Subsequently, significant repulsive interactions between CO_2 and the GO layers prevent CO_2 from migrating from its original position. Such repulsive interactions cannot occur in anhydrous GO structures because the anhydrous structures have larger interlayer spacing. In this case, carbon dioxide can easily migrate in the interlayer space of double GO layers to exit the

structure. Consequently, the spacing of the GO layers, which are connected by water molecules through hydrogen bonds, determines the carbon dioxide migration kinetics. The DFT findings are helpful for understanding the mechanisms of trapping carbon dioxide molecules in the interlayer space of hydrated graphene oxides and for designing nanocarbon materials as promising candidates for capturing greenhouse gases.

Electronic supplementary information (ESI) available: Dependence of total energy of $C_{64}O_4(OH)_{16} \cdot 4H_2O$ on *k*-point meshes (S1); Cartesian coordinates of optimised geometries in Figure 2 (S2); Cartesian coordinates of optimised geometries in Figure 3 (S3); Cartesian coordinates of optimised geometries in Figure 4; S5 Cartesian coordinates of optimised geometries in Figure 5 (S4); Cartesian coordinates of optimised geometries in Figure 7 (S6); Cartesian coordinates of transition states for CO_2 migration within graphene oxide models in Figure 10 (S7); Complete lists in Ref. 58 (S8). See DOI:XXX.

References and Notes

1 B. Brodie, *Ann. Chim. Phys.*, 1855, **45**, 351.

2 B. Brodie, *Philos. Trans. R. Soc. London,* 1859, **A149**, 249.

3 U. Hofmann and R. Holst, *Ber. Dtsch. Chem. Ges.*, 1939, **72**, 754.

4 G. Ruess, *Monatsch. Chem.*, 1946, **76**, 381.

5 A. Clauss, R. Plass, H.-P. Boehm and U. Hofmann, *Z. Anorg. Allg. Chem.*, 1957, **291**, 205.

6 W. Scholz and H.-P. Boehm, *Anorg. Allg. Chem.*, 1969, **369**, 327.

7 T. Nakajima, T. Mabuchi and R. Hagiwara, *Carbon*, 1988, **26**, 357.

8 T. Nakajima and Y. Matsuo, *Carbon*, 1994, **32**, 469.

9 D. R. Dreyer, S. Park, C. W. Bielawski and R. S. Ruoff. *Chem. Soc. Rev.* 2010, **39**, 228.

10 Y. Zhu, S. Murali, W. Cai, X. Li, J. W. Suk, J. R. Potts and R. S. Ruoff, *Adv. Mater.* 2010, **22**, 3906.

11 S. Mao, H. Pu, and J. Chen, *RSC Adv.*, 2012, **2**, 2643.

12 V. C. Tung, M. J. Allen, Y. Yang and R. B. Kaner, *Nature Nanotech.*, 2009, **4**, 25.

13 S. Park and R. S. Ruoff, *Nature Nanotech.*, 2009, **58**, 217.

14 Z. Wei, D. Wang, S. Kim, S.-Y. Kim, Y. Hu, M. K. Yakes, A. R. Laracuente, Z. Dai, S. R. Marder, C. Berger, W. P. King, W. A. de Heer, P. E. Sheehan and E. Riedo, *Science*, 2010, **328**, 1373.

15 C. Mattevi, G. Eda, S. Agnoli, S. Miller, K. A. Mkhoyan, O. Celik, D. Mastrogiovanni, G. Granozzi, E. Grafunkel and M. Chhowalla, *Adv. Funct. Mater.*, 2009, **19**, 2577.

16 D. A. Dikin, S. Stankovich, E. J. Zimney, R. D. Piner, G. H. B. Dommett, G. Evmenenko, S. T. Nguyen and R. Ruoff, *Nature*, 2007, **448**, 457.

17 P. Johari and V. B. Shenoy, *ACS Nano*, 2011, **5**, 7640.

18 G. Eda, G. Fanchini and M. Chhowalls, *Nature Nanotech.*, 2008, **3**, 270.

19 X. Wu, M. Sprinkle, X. Li, F. Ming, C. Berger and W. A. der Heer, *Angew. Chem. Int. Ed.*, 2008, **101**, 026801.

20 J. T. Robinson, M. Zalautdinov, J. W. Baldwin, E. S. Snow, Z. Wei, P. Sheehan and B. H. Houston, *Nano Lett.*, 2008, **8**, 3441.

21 J. T. Robinson, F. K. Perkins, E. S. Snow, Z. Wei and P. Sheehan, *Nano Lett.*, 2008, **8**, 3137.

22 A. Lerf, H. He, M. Forster and J. Klinowski, *J. Phys. Chem. B*, 1998, **102**, 4477.

23 T. Szabó, O. Berkesi, P. Forgo, K. Josepovits, Y. Sanakis, D. Petridis and I. Dékány, *Chem. Mater.*, 2006, **18**, 2740.

24 H.-K. Jeong, Y. P. Lee, R. J. W. E. Lahaye, M.-H. Park, K. H. An, I. J. Kim, C.-W. Yang, C. Y. Park, R. S. Ruoff and Y. H. Lee, *J. Am. Chem. Soc.* 2008, **130**, 1362.

25 K. N. Kudin, B. Ozbas, H. C. Schniepp, R. K. Pru'homme, I. A. Aksay and R. Car, *Nano Lett.*, 2008, **8**, 36.

26 K. A. Mkhoyan, A. W. Contryman, J. Silcox, D. A. Stewart, G. Eda, C. Mattevi, S. Miller and M. Chhowalla, *Nano Lett.,* 2009, **9**, 1058.

27 W. Gao, L. B. Alemany, L. Ci and P. M. Ajayan, *Nature Chem.*, 2009, **1**, 403.

28 L. B. Casabianca, M. A. Shaibat, W. W. Cai, S. Park, R. Piner, R. S. Ruoff and Y. Ishii, *J. Am. Chem. Soc.*, 2010, **132**, 5672.

29 C. Gómez-Navarro, J. C. Mayer, R. S. Sundaram, A. Chuvilin, S. Kurasch, M. Burghard, K. Kern and U. Kaiser, *Nano Lett.*, 2010, **10**, 1144.

30 K. Erickson, R. Erni, Z. Lee, N. Alem, W. Gannett and A. Zettl, *Adv. Mater.*, 2010, **22**, 4467.

31 J. P. Rourke, P. A. Pandey, J. J. Moore, M. Bates, I. A. Kinloch, R. J. Young and N. R. Wilson, *Angew. Chem. Int. Ed.*, 2011, **50**, 3173.

32 D. Pacilé, J. C. Meyer, A. F. Rodríguez, M. Papagno, C. Gómez-Navarro, R. S. Sundaram, M. Burghard, K. Kern, C. Carbone and U. Kaiser, *Carbon*, 2011, **49**, 966.

33 S. Kim, S. Zhou, Y. Hu, M. Acik, Y. J. Chabal, C. Berger, W. de Heer, A. Bongiorno and E. Riedo, *Nature Mater.*, 2012, **11**, 544.

34 A. Dimiev, D. V. Kosynkin, L. B. Alemany, P. Chaguine and J. M. Tour, *J. Am. Chem. Soc.*, 2012, **134**, 2815.

35 L. R. de Jesus, R. V. Dennis, S. W. Depner, C. Jaye, D. A. Fischer and S. Banerjee, *J. Phys. Chem. Lett.*, 2013, **4**, 3144.

36 A. Lerf, A. Buchsteiner, J. Pieper, S. Schöttl, I. Dekany, T. Szabo and H. P. Boehm, *J. Phys. Chem. Solid*, 2006, **67**, 1106.

37 M. Aclik, C. Mattevi, C. Gong, G. Lee, K. Cho, M. Chhowall and Y. J. Chabal, *ACS Nano*, 2010, 5861.

38 N. V. Medhekar, A. Ramasubramaniam, R. S. Ruoff and V. B. Shenoy, *ACS Nano*, 2010, **4**, 2300.

39 L. Wang, K. Lee, Y.-Y. Sun, M. Lucking, Z. Chen, J. J. Zhao and S. B. Zhang, *ACS Nano*, 2009, **3**, 2995.

40 B. H. Kim, W. G. Hong, H. Y. Yu, Y.-K. Han, S. M. Lee, S. J. Chang, H. R. Moon, Y. Jun and H. J. Kim, *Phys. Chem. Chem. Phys.*, 2012, **14**, 1480.

41 S. Eigler, C. Dotzer, A. Hirsch, M. Enzelberger and P. Müller, *Chem. Mater.*, 2012, **24**, 1276.

42 J.-L. Li, K. N. Kudin, M. J. McAllister, R. K. Prud'homme, I. A. Aksay and R. Car, *Phys. Rev. Lett.*, 2006, **96**, 176101.

43 H. C. Schniepp, J.-L. Li, M. J. McAllister, H. Sai, M. Herrera-Alonso, D. H. Adamson, R. K. Prud'homme, R. Car, D. A. Saville and I. A. Aksay, *J. Phys. Chem. B*, 2006, **110**, 8535.

44 J. T. Paci, T. Belytschko and G. C. Schatz, *J. Phys. Chem. C*, 2007, **111**, 18099.

45 D. W. Boukhvalov and M. I. Katsnelson, *J. Am. Chem. Soc.*, 2008, **130**, 10697.

46 J.-A. Yan, L. Xian and M. Y. Chou, *Phys. Rev. Lett.* 2009, **103**, 086802.

47 R. J. W. E. Lahaye, H. K. Jeong, C. Y. Park and Y. H. Lee, *Phys. Rev. B*, 2009, **79**, 125435.

48 W. Zhang, V. Carravetta, Z. Li, Y. Luo and J. Yang, *J. Chem. Phys.*, 2009, **131**, 244505.

49 A. Bagri, C. Mattevi, M. Acik, Y. J. Chabal, M. Chhowalla and V. B. Shenoy, *Nature Chem.* 2010, **2**, 581.

50 D. L. Duong, G. Kim, H.-K. Jeong and Y. H. Lee, *Phys. Chem. Chem. Phys.* 2010, **12**, 1595.

51 H. J. Xiang, S.-H. Wei and X. G. Gong, *Phys. Rev. B*, 2010, **82**, 035416.

52 J.-A. Yan and M. Y. Chou, *Phys. Rev. B*, 2010, **82**, 125403.

53 L. Wang, Y. Y. Sun, K. Lee, D. West, Z. F. Chen, J. J. Zhao, and S. B. Zhang, *Phys. Rev. B*, 2010, **82**, 161406(R).

54 R. Larciprete, S. Fabris, T. Sun, P. Lacovig, A. Baraldi and S. Lizzit, *J. Am. Chem. Soc.*, 2011, **133**, 17315.

55 T. Sun, S. Fabris and S. Baroni, *J. Phys. Chem. C* 2011, **115**, 4730.

56 R. M. Abolfath and K. Cho, *J. Phys. Chem. A*, 2012, **116**, 1820.

57 S. Zhou, S. Kim and A. Bongiorno, *J. Phys. Chem. C*, 2013, **117**, 6267.

58 M. J. Frisch, et al. Gaussian 09, Gaussian Inc.; Wallingfold, CT, 2009.

59 J. P. Perdew, K. Burke and M. Ernzerhof, *Phys. Rev. Lett.*, 1996, **77**, 3865.

60 S. Grimme, *J. Comput. Chem.* 2006, **27**, 1787.

61 W. J. Hehre, R. Ditchfield and J. A. Pople, *J. Chem. Phys.* 1972, **56**, 2257.

62 R. Krishnan, J. S. Binkley, R. Seeger and J. A. Pople, *J. Chem. Phys.* 1980, **72**, 650.

63 S. F. Boys and F. Bernardi, *Mol. Phys*. 1970, **19**, 553.

64 L. A. Curtiss, D. J. Frurip, M. Blander, *J. Chem. Phys.*,1979, **71**, 2703. This reference reported an experimental $E_{interact}$ value being –5.44 ± 0.7 kcal/mol.

65 J. Ireta, J. Neugebauer and M. Scheffler, *J. Phys. Chem. A*, 2004, **108**, 5692.

66 Y. Zhao and D. G. Truhlar, *J. Chem. Theory Comput.*, 2005, **1**, 415.

67 L. Rao, H. Ke, G. Fu, X. Xu and Y. Yan, *J. Chem. Theory Comput.*, 2009, **5**, 86.

68 To investigate interactions of water (carbon dioxide) with a single GO through hydrogen bonding, we considered two types of basis-set combination. In one type, we used the 6-31G** basis set for all atoms, and in the other type we used the 6-31++G** basis set for water (carbon dioxide) and attached OH groups, and the 6-31G** basis set for the other atoms.

69 With respect to interactions of water with a GO, Table 2 shows that the HOH···OH separations obtained in the PBE/6-31G** and B97D/6-31G**calculations are similar; the PBE (B97D) calculations yield separations of 2.17 and 2.60 (2.26 and 2.69) Å. Similar $E_{interact}$ values were found in the PBE/6-31G** and B97D/6-31G**calculations, being approximately –4.0 and –2.0 kcal/mol, respectively.

70 (a) T. Yumura, K. Hirahara, S. Bandow, K. Yoshizawa and S. Iijima, *Chem. Phys. Lett.,* 2004, **386**, 38. (b) T. Yumura, S. Bandow, K. Yoshizawa and S. Iijima, *J. Phys. Chem.* B, 2004, **108**, 11426. (c) T. Yumura, D. Nozaki, S. Bandow, K. Yoshizawa and S. Iijima, *J. Am. Chem. Soc.*, 2005, **127**, 11769. (d) T. Yumura, M. Kertesz and S. Iijima, *J. Phys. Chem. B*, 2007, **111**, 1099. (e) T. Yumura, M. Kertesz and S. Iijima, *Chem. Phys. Lett.,* 2007, **444**, 155. (f) T. Yumura and M. Kertesz, *J. Phys. Chem. C*, 2009, **113**, 14184. (g) T. Yumura, *Phys. Chem. Chem. Phys.*, 2011, **13**, 337. (h) H. Yamashita and T. Yumura, *J. Phys. Chem. C*, 2012, **116**, 9681. (i) T. Yumura and H. Yamashita, *J. Phys. Chem. C*, 2014, **118**, 5510.

71 In terms of the dependences of the interlayer spacings on [O]/[C] in graphene oxides, the trends in the PBE calculations can be reproduced by dispersion-corrected B97D

calculations. The B97D-calculated interlayer spacings of $C_{32}(OH)_2$, $C_{16}(OH)_2$, $C_{32}(OH)_4$, $C_{32}(OH)_4$, $C_{32}(OH)_6$, $C_{16}(OH)_4$, and $C_{16}(OH)_6$ are 5.32, 5.12, 5.23, 6.10, 6.40, and 7.69 Å, respectively.

72 Natural population analyses (NPA) revealed that charges of oxygen atoms in epoxy and hydroxyl groups were –0.6 and –0.7, respectively.

73 L. Liu, L. Wang, J. Gao, J. Zhao, H. Gao and Z. F. Chen, *Carbon*, 2012, **50**, 1690.

74 Note that the energy difference would be influenced by the positions of the functional groups due to the occurrence of interlayer hydrogen-bonding interactions. Thus, the DFT calculations do not indicate that the anhydrous GO structures have AA stacking. In fact, some TEM observations show turbostatic stacking behaviour. See Ref. 30 and the following reference: N. R. Wilson, P. A. Pandey, R. Beanland, R. J. Young, I. A. Kinloch, L. Gong, Z. Liu, K. Suenaga, J. P. Rourke, S. J. York and J. Sloan, *ACS Nano*, 2009, **3**, 2547.

75 In the evaluating of the activation energies (E_a) for CO_2 migration within a graphene oxide, we fixed the $C_{64}O_4(OH)_{16}\cdot nH_2O$ structure to that taken from the local minimum of $CO_2@C_{64}O_4(OH)_{16}\cdot nH_2O$ by removing CO_2. To obtain further proper understanding of the activation energy, we relaxed coordinates of attached groups (OH or O groups) and H_2O molecules in the transition states (Figure 10), however those of other atoms are fixed. The activation energies for the CO_2 migration within the partially relaxed $CO_2@C_{64}O_4(OH)_{16}\cdot nH_2O$ are 7.9, 24.7, and 37.4 kcal/mol for n = 0, 1, and 2, respectively. The E_a values are similar to those obtained by using the fixed $C_{64}O_4(OH)_{16}\cdot nH_2O$ geometries.

Figure Captions

Figure 1. Supercells of double graphene layers, which are used to construct graphene oxides; (a) a supercell containing 16 red atoms (2×2×2 cell), (b) a supercell containing 32 atoms (16 red and 16 blue atoms) (2×4×2 cell), and (c) a supercell containing 64 atoms (16 red, 16 blue, and 32 green atoms) (4×4×2 cell). Graphene models with AA or AB stacking were used as the initial geometries to obtain optimised double-layered graphene oxides. Lattice vectors are given.

Figure 2. (a) Optimised structures for a water dimer with C_s symmetry were obtained from the PBE/6-31G** and B97D/6-31G** calculations. In the optimised structures, an H atom of a water molecule binds to the oxygen atom of the other water molecule through hydrogen bonds (the HOH··OH separation). Dependences of the separations on basis sets are tabulated in Table 1. Optimised structure for a single graphene oxide attached by one water molecule (b) or one carbon dioxide (c), obtained from the PBE/6-31G** and B97D/6-31G** calculations. The unit cell contains eight carbon atoms and two hydroxyl groups. There are hydrogen bonds between the water and the single GO layer (HOH··OH separations), and between the carbon dioxide and the GO layer (OCO··HO separations). Dependences of the separations on basis sets are tabulated in in Table 2.

Figure 3. Optimised structures for graphene oxides consisting of smaller supercells (2×2×2 or 2×4×2 cell) with a few attached hydroxyl groups. (a) $C_{16}(OH)_2$, (b)

$C_{16}(OH)_4$, (c) $C_{16}(OH)_6$, (d) $C_{32}(OH)_2$, (e) $C_{32}(OH)_4$ and (f) $C_{32}(OH)_6$. Water oxygen atoms, oxygen atoms attached on graphene layers, graphene carbon atoms, and hydrogen atoms are represented by green, red, blue, and grey balls, respectively. Filled balls represent atoms in the supercell, and hollow balls represent atoms located in neighbouring supercells. Their optimised interlayer spacings are given in Å**.** Hydrogen bonds are represented by dotted lines. The ratios of the number of oxygen atoms to that of carbon atoms are given.

Figure 4. We quadrupled the $C_{16}O(OH)_4 \cdot H_2O$ structure to create the $C_{64}O_4(OH)_{16} \cdot 4H_2O$ structure. (a) Side view of the optimised $C_{64}O_4(OH)_{16} \cdot 4H_2O$ structure. Water oxygen atoms, oxygen atoms attached on graphene layers, graphene carbon atoms, and hydrogen atoms are represented by green, red, blue, and grey balls, respectively. Filled balls represent atoms in the supercell, and hollow balls represent atoms located in neighbouring supercells. Hydrogen bonds are represented by dotted lines. (b) Top view of the optimised $C_{64}O_4(OH)_{16} \cdot 4H_2O$ structure. Atoms on the top layer are represented by filled balls, and those on the bottom layer are represented by hollow balls. (c) The four intercalated water molecules, taken from the optimised structure, are depicted.

Figure 5. Optimised structures for anhydrous and hydrated graphene oxides ($C_{64}O_4(OH)_{16} \cdot nH_2O$) obtained from the PBE calculations. (a) Side views of the optimised structures. Their interlayer spacings are displayed in Å. Water oxygen

atoms, oxygen atoms attached on graphene layers, graphene carbon atoms, and hydrogen atoms are represented by green, red, blue, and grey balls, respectively. Filled balls represent atoms in the supercell, and hollow balls represent atoms located in neighbouring supercells. Hydrogen bonds are represented by dotted lines. (b) Top views of the optimised structures. Atoms on the top layer are represented by filled balls, and those on the bottom layer are represented by hollow balls.

Figure 6. Variations in the interlayer spacings (Å) of $C_{64}O_4(OH)_{16}\cdot nH_2O$ and $CO_2@C_{64}O_4(OH)_{16}\cdot nH_2O$ as a function of the number of water molecules in the structure. Blue dots represent the interlayer spacing of $C_{64}O_4(OH)_{16}\cdot nH_2O$, and red dots represent that of $CO_2@C_{64}O_4(OH)_{16}\cdot nH_2O$.

Figure 7. Optimised structures for anhydrous and hydrated graphene oxides ($CO_2@C_{64}O_4(OH)_{16}\cdot nH_2O$) obtained from the PBE calculations. (a) Side views of the optimised structures. Their interlayer spacings are displayed in Å. Water oxygen atoms, oxygen atoms attached on graphene layers, graphene carbon atoms, CO_2 carbon atoms, and hydrogen atoms are represented by green, red, blue, purple, and grey balls, respectively. Filled balls represent atoms in the supercell, and hollow balls represent atoms located in neighbouring supercells. (b) Top views of the optimised structures. Atoms on the top layer are represented by filled balls, and those on the bottom layer are represented by hollow balls.

Figure 8. CO_2 migration along the $a_1 + a_2$ vector from its original position in $CO_2@C_{64}O_4(OH)_{16}\cdot nH_2O$. The migration is projected on the bottom layer by removing the top of layer of an optimised $CO_2@C_{64}O_4(OH)_{16}\cdot nH_2O$ structure. The degree of migration of carbon dioxide from its original position is given by T. The structures at $T = 0$ correspond to the optimised $C_{64}O_4(OH)_{16}\cdot nH_2O$ structures.

Figure 9. Energy profiles of the migration of carbon dioxide within the $C_{64}O_4(OH)_{16}\cdot nH_2O$ structures. T, the degree of migration of carbon dioxide from its original position, is defined in Figure 8. Energies of CO_2 migration in the interlayer spaces of $C_{64}O_4(OH)_{16}\cdot 2H_2O$, $C_{64}O_4(OH)_{16}\cdot H_2O$, and $C_{64}O_4(OH)_{16}$ structures are represented by blue, green, and red marks, respectively. Energy barriers of migration of carbon dioxide within anhydrous and hydrated graphene oxides (E_a) were obtained; 44.0 kcal/mol for $C_{64}O_4(OH)_{16}\cdot 2H_2O$, 28.0 kcal/mol for $C_{64}O_4(OH)_{16}\cdot H_2O$, and 8.4 kcal/mol for $C_{64}O_4(OH)_{16}$.

Figure 10. Transition states of CO_2 migration within $C_{64}O_4(OH)_{16}\cdot nH_2O$ structures. (a) Top views of transition states, whose top layer is removed, and their side views. Water oxygen atoms, oxygen atoms attached on graphene layers, graphene carbon atoms, CO_2 carbon atoms, and hydrogen atoms are represented by green, red, blue, purple, and grey balls, respectively. Key oxygen separations between carbon dioxide and attached hydroxyl groups are given in Å.

Table 1. Accuracy of density functional theory calculations in describing the hydrogen-bonding interactions that occurred in the water dimer in Figure 2.

		Method / Basis sets			
		PBE/6-31G**	PBE /6-31++G**	B97D/6-31G**	B97D /6-31++G**
H_2O dimer	$E_{interact}$ [1)]	−5.5	−5.5	−4.9	−4.8
	HOH··OH [2)]	1.91	1.91	1.97	1.95

1) $E_{interact}$(kcal/mol); interaction energy by binding of a water molecule to the other water molecule. $E_{interact}$ is defined by E_{total}(water dimer) – 2 E_{total}(water monomer), where E_{total}(water dimer) is the total energy of the optimized water dimer, and E_{total}(water monomer) is that of the optimized water monomer. Then, BSSEs in E_{total}(water dimer) were corrected according to Ref. 63. Negative $E_{interact}$ values indicate that attractive interactions occur in the water dimer or between water and graphene oxide.

2) HOH··OH (Å); separation between an acceptor H atom and a donor O atom in hydrogen bond formation.

Table 2. Accuracy of density functional theory calculations in describing the hydrogen-bonding interactions that occurred between water and graphene oxide (H_2O–GO) and between carbon dioxide and graphene oxide (CO_2–GO) in Figure 2.

		Method / Basis sets			
		PBE/6-31G**	PBE /6-31++G**+6-31G** [5)]	B97D/6-31G**	B97D /6-31++G**+6-31G** [5)]
H_2O–GO	$E_{interact}$ [1)]	−4.1	−3.7	−2.0	−2.1
	HOH··OH [2)]	2.17, 2.14, 2.60	2.12, 2.29, 2.58	2.26, 2.31, 2.68	2.28, 2.42, 2.92
CO_2–GO	$E_{interact}$ [3)]	−0.3	−0.8	0.2	0.0
	OCO··HO [4)]	2.80, 2.86, 2.94, 3.00	2.85, 2.88, 3.11, 3.13	3.10, 3.15, 3.21, 3.25	3.22, 3.37, 3.38, 3.51

1) $E_{interact}$ (kcal/mol); interaction energy by binding a water molecule to a single graphene-oxide layer. $E_{interact}$ is defined by E_{total}(H_2O–GO) – E_{total}(GO) – E_{total}(H_2O), where E_{total}(H_2O–GO) is the total energy of the optimized structure for H_2O binding into a single GO, E_{total}(GO) is that of the optimized GO structure, and E_{total}(H_2O) is that of the optimized water molecule. Then, BSSEs in E_{total}(H_2O–GO) were corrected according to Ref. 63. Negative $E_{interact}$ values indicate that attractive interactions occur in the water dimer or between water and graphene oxide.

2) HOH··OH (Å); separation between an acceptor H atom and a donor O atom in hydrogen bond formation.

3) $E_{interact}$ (kcal/mol); interaction energy by binding a carbon dioxide molecule to a single graphene-oxide layer. $E_{interact}$ is defined by E_{total}(CO_2–GO) – E_{total}(GO) – E_{total}(CO_2), where E_{total}(CO_2–GO) is the total energy of the optimized structure for CO_2 binding into a single GO, E_{total}(GO) is that of the optimized GO structure, and E_{total}(CO_2) is that of the optimized structure for CO_2 molecule. Then, BSSEs in E_{total}(CO_2–GO) were corrected according to Ref. 63. Negative $E_{interact}$ values indicate that attractive interactions occur in the water dimer or between water and graphene oxide.

4) OCO··HO (Å); separation between an acceptor H atom of an attached OH group and a donor O atom of CO_2 in hydrogen bond formation.

5) The 6-31++G** basis set was used for water (carbon dioxide) and attached OH groups, and the 6-31G** basis set was used for the other atoms.

Table 3. Optimised interlayer spacings of graphene oxides in PBE calculations in Figure 3.

Structure labels	[O]/[C] [1)]	Oxygen-containing groups	Interlayer spacing[2)]
$C_{32}(OH)_2$	0.063	OH	5.07
$C_{16}(OH)_2$	0.125	OH	4.92
$C_{32}(OH)_4$	0.125	OH	5.03
$C_{32}(OH)_6$	0.188	OH	5.71
$C_{16}(OH)_4$	0.250	OH	5.95
$C_{16}(OH)_6$	0.375	H_2O, OH, O	7.05

1) [O]/[C]; ratio of the number of oxygen atoms to that of carbon atoms.

2) Interlayer spacings in Å

Table 4. Energetics of the optimised $C_{64}O_4(OH)_{16}\cdot nH_2O$ and $CO_2@C_{64}O_4(OH)_{16}\cdot nH_2O$ structures.

		n				
	CO_2	0	1	2	3	4
E(*l*–*l*) [1)]	Absence	–7.2	–4.8	–4.0	–1.4	–1.2
E(*w*–*l*) [2)]	Absence	–	–10.9	–7.7	–9.3	–9.1
Interlayer spacing	Absence	5.87	6.42	6.71	7.00	7.08
E(*l*–*l*) [1)]	presence	0.3	0.5	0.6	0.3	–
E(*w*–*l*) [2)]	presence	–	–10.5	–10.1	–9.8	–
E (CO_2–*l*) [3)]	presence	–2.7	0.1	2.0	4.1	–
Interlayer spacing	presence	8.45	7.90	7.70	7.65	–

1) E(*l*–*l*) (kcal/mol); interlayer interactions defined in Eq. (1). Negative values indicate attractive interactions.

2) E(*w*–*l*) (kcal/mol); interactions of one water molecule with a double-layered graphene oxide, defined in Eq. (2). Negative values indicate attractive interactions.

3) *E*(CO_2–*l*) (kcal/mol); interactions of carbon dioxide with a double-layered graphene oxide, defined in Eq. (3). Negative values indicate attractive interactions.

Table of contents entry

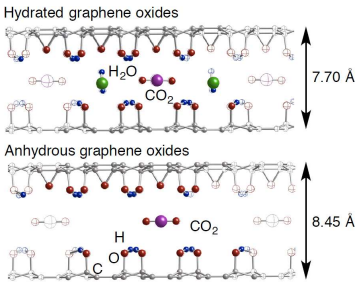

DFT calculations revealed that migration of CO_2 within graphene oxides is influenced by the presence or absence of intercalated waters.